

Ionization of hydrogen by neutrino magnetic moment, relativistic muon, and WIMPJiunn-Wei Chen,^{1,2} C.-P. Liu,³ Chien-Fu Liu,¹ and Chih-Liang Wu¹¹*Department of Physics and Center for Theoretical Sciences, National Taiwan University, Taipei 10617, Taiwan*²*National Center for Theoretical Sciences and Leung Center for Cosmology and Particle Astrophysics, National Taiwan University, Taipei 10617, Taiwan*³*Department of Physics, National Dong Hwa University, Shoufeng, Hualien 97401, Taiwan*

(Received 11 July 2013; published 19 August 2013)

We studied the ionization of hydrogen by the scattering of the neutrino magnetic moment, relativistic muon, and a weakly interacting massive particle with a QED-like interaction. Analytic results were obtained and compared with several approximation schemes often used in atomic physics. As current searches for the neutrino magnetic moment and dark matter have lowered the detector threshold down to the sub-keV regime, we tried to deduce from this simple case study the influence of the atomic structure on the cross sections and the applicabilities of various approximations. The general features being found will be useful for cases where practical detector atoms are considered.

DOI: [10.1103/PhysRevD.88.033006](https://doi.org/10.1103/PhysRevD.88.033006)

PACS numbers: 14.60.Lm, 13.15.+g, 32.80.-t, 95.35.+d

I. INTRODUCTION

The electromagnetic (EM) properties of neutrinos, in particular, the magnetic dipole moments μ_ν , are of fundamental importance not only in particle physics but also astrophysics and cosmology (for reviews see, e.g., Refs. [1,2]). In the Standard Model with massive neutrinos, a nonvanishing μ_ν arises as a result of the one-loop electroweak radiative correction; for Dirac neutrinos,¹ it is given by $\mu_\nu = 3.20 \times 10^{-19} (\frac{m_\nu}{\text{eV}}) \mu_B$, where the Bohr magneton $\mu_B = e/(2m_e)$ with e and m_e being the magnitude of charge and mass of electron.² From the current mass upper limit set on the electron neutrino in the tritium β decay [3], $m_{\nu_e} < 2$ eV, one can estimate that $\mu_{\nu_e} \lesssim 10^{-18} \mu_B$ is indeed very tiny in the Standard Model.

The best direct limits on μ_ν so far are extracted mostly from neutrino-electron (νe) scattering: with the reactor antineutrinos, $\mu_{\bar{\nu}_e} < 2.9 \times 10^{-11} \mu_B$ by the GEMMA Collaboration [4] and $\mu_{\bar{\nu}_e} < 7.4 \times 10^{-11} \mu_B$ by the TEXONO Collaboration [5], with the solar neutrinos, $\mu_{\nu_\odot} < 5.4 \times 10^{-11} \mu_B$ by the Borexino Collaboration [6]. Many stronger, but indirect, limits ranging from 10^{-11} to $10^{-13} \mu_B$ were inferred from astrophysical or cosmological constraints; however, they are subject to model dependence and theoretical uncertainty. Because the current limits, whether direct or indirect, are orders of magnitude away from the Standard Model prediction, it makes the search of μ_ν a powerful probe of new physics.

The cross section of neutrino scattering off a free electron through the EM interaction with μ_ν is [7]

$$\frac{d\sigma}{dT} \Big|_{\text{FE}} = 4\pi\alpha\mu_\nu^2 \left(\frac{1}{T} - \frac{1}{E_\nu} \right), \quad (1)$$

where α is the fine structure constant, E_ν the neutrino incident energy, and T the neutrino energy deposition. The $1/T$ feature indicates a way of improving the limit on μ_ν by lowering the detector threshold of T . Currently the thresholds can be as low as a few keV (e.g., the germanium semiconductor detectors deployed by both the GEMMA and TEXONO Collaborations), and the next-generation detectors are geared up to extend down to the sub-KeV regime [8,9]. While one expects improved limits from such experimental upgrades, a theoretical issue regarding how the electronic structure of detectors affects the simple free νe scattering formula naturally arises, as the associated energy scale is comparable to the atomic scale. Recently there have been discussions about whether the atomic structure can possibly enhance an atomic ionization (AI) cross section [10,11] and the robustness of a free electron approximation in low energy transfer [12,13]. While experiments keep pushing down the detector threshold, the need for more reliable cross section formulas will certainly grow.

Another type of experiment where AI can be relevant is the search for dark matter (DM), as it shares many similar detection techniques as for μ_ν . Most current search focus on the weakly interacting massive particles (WIMPs) with masses about GeV to TeV scales – favoured for astrophysical reasons – with nuclear recoil in targets being the main observable. Recently, the sub-GeV DM candidates, generically classified as light dark matter, have started to get attention [14], and the associated AI processes in targets can be used to constrain the interaction of light dark matter candidates with electrons and their masses [15].

Given the importance of understanding the detectors' response, in particular, in the low energy regime, our study starts by considering the simplest atom, hydrogen. By

¹Note that both Dirac and Majorana neutrinos can acquire “transition” magnetic dipole moments by similar one-loop radiative corrections in the Standard Model. In this article we concentrate on the “static” ones, which only Dirac neutrinos can have.

²In this article, we adopt the natural units $c = \hbar = 1$.

treating the electrons as nonrelativistic particles and including the one photon exchange together with the Coulomb interaction, the problem is solved analytically with $O(v_e^2)$ and $O(\alpha^2)$ errors, where v_e is the electron velocity. We then compare our result against various widely used approximation schemes for the AI through μ_ν or DM scattering; we try to draw useful information about the applicabilities of these approximation schemes under various kinematic conditions. This knowledge serves as a precursor to our currently ongoing projects with realistic atomic species.

The article is organized as follows: In Sec. II, we lay down the general formalism for AI cross sections through EM interactions. The analytic results for the atomic response functions of hydrogenlike atoms are given explicitly, and approximation schemes including the free electron approximation (FEA), equivalent photon approximation (EPA), longitudinal photon approximation (LPA), and the one of Kouzakov-Studenikin-Voloshin (KSV) [13] are introduced. The case of AI by μ_ν is studied in Sec. III, with particular attention to the issue of whether the atomic structure enhances or suppresses the cross sections while scattering occurs at atomic scales. In Sec. IV, the well-known AI process by a relativistic muon is revisited. A detailed account of why EPA works for this case but not for μ_ν is given. Finally, we extend the above formalism to a QED-like gauge model for the DM interaction with normal matter, and study the hydrogenic response under various DM kinematics in Sec. V. A brief summary is in Sec. VI.

II. FORMALISM

Consider the ionization of a hydrogenlike atom H by a lepton l ,

$$l + \text{H} \rightarrow l + \text{H}^+ + e^-, \quad (2)$$

through one photon exchange, as shown in Fig. 1. We will treat the electron as a nonrelativistic particle and include all its Coulomb interactions in the initial and final states. This problem can be solved analytically. The results will be referred as the “full” ones—in comparison to various

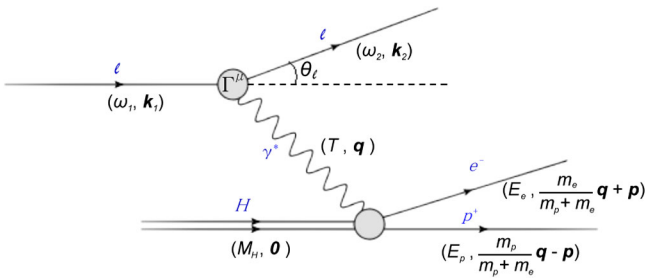


FIG. 1 (color online). The atomic ionization process $l + \text{H} \rightarrow l + \text{H}^+ + e^-$ through one photon exchange in the laboratory frame.

approximations to be discussed later on—and have errors on the order of $O(v_e^2, \alpha^2)$.

The unpolarized differential cross section in the laboratory frame, i.e., the velocity of the incident lepton $\vec{v}_l \neq 0$ and the velocity of the atomic target $\vec{v}_\text{H} = 0$, is expressed as³

$$d\sigma = \frac{1}{|\vec{v}_l|} \frac{(4\pi\alpha)^2}{Q^4} \bar{l}^{\mu\nu} \bar{W}_{\mu\nu} (2\pi)^4 \delta^4(k_1 + p_\text{H} - k_2 - p_R - p_r) \times \frac{d^3\vec{k}_2}{(2\pi)^3} \frac{d^3\vec{p}_R}{(2\pi)^3} \frac{d^3\vec{p}_r}{(2\pi)^3}, \quad (3)$$

where the four momenta $k_1 = (\omega_1, \vec{k}_1)$ and $k_2 = (\omega_2, \vec{k}_2)$ are of the initial and final leptons, $p_\text{H} = (M_\text{H}, \vec{0})$ of the initial atom, $p_R = (E_R, \vec{p}_R)$ and $p_r = (E_r, \vec{p}_r)$ of the final $\text{H}^+ + e^-$ state in the center-of-mass and relative coordinates, and $q^\mu = k_1^\mu - k_2^\mu = (T, \vec{q})$ of the virtual photon, respectively, and $Q^2 = q_\mu q^\mu$. The leptonic tensor,

$$\bar{l}^{\mu\nu} \equiv \sum_{s_2} \overline{\sum_{s_1}} \langle k_2, s_2 | j_l^\mu | k_1, s_1 \rangle \langle k_2, s_2 | j_l^\nu | k_1, s_1 \rangle^*, \quad (4)$$

is obtained by a sum of the final spin state s_2 and an average of the initial spin state s_1 of the leptonic EM current j_l matrix elements; and similarly the atomic tensor,

$$\bar{W}^{\mu\nu} \equiv \sum_{m_{jf}} \overline{\sum_{m_{ji}}} \langle f | j_A^\mu | i \rangle \langle f | j_A^\nu | i \rangle^*, \quad (5)$$

involves a sum of the final angular momentum state m_{jf} and an average of the initial angular momentum state m_{ji} of the atomic EM current j_A matrix elements, where $|i\rangle$ and $|f\rangle$ refer to atomic initial and final states, respectively.

In this work, we use the relativistic form for j_l^μ ,

$$\langle k_2, s_2 | j_l^\mu | k_1, s_1 \rangle = \bar{u}(k_2, s_2) \left[F_1^{(l)} \gamma^\mu - i \frac{F_2^{(l)}}{2m_e} \sigma^{\mu\nu} q_\nu \right] u(k_1, s_1). \quad (6)$$

The Dirac and Pauli form factors, $F_1^{(l)}$ and $F_2^{(l)}$, which describe the helicity-preserving and helicity-changing EM couplings, are constant for elementary leptons: $F_1^{(l)}$ is the charge e_l (in units of e) and $F_2^{(l)}$ the anomalous magnetic dipole moment κ_l (in units of μ_B).

Since we are only interested in the case that the energy deposition by the incident particle is small enough such that electrons can be treated as nonrelativistic particles, the charge and spatial current densities in momentum space are

$$\rho^{(A)}(\vec{q}) = -e^{i\vec{q} \cdot (\vec{R} + \vec{r})}, \quad (7)$$

³We adopt the normalization $u^\dagger u = 1$ for all Dirac spinors.

$$\vec{j}^{(A)}(\vec{q}) = \frac{-1}{2m_e} e^{i\vec{q}\cdot(\vec{R}+\vec{r})}(\vec{q} + 2\vec{p}_r + i\vec{\sigma}_e \times \vec{q}). \quad (8)$$

$\rho^{(A)}$ is leading in the $1/m_e$ expansion while $\vec{j}^{(A)}$ is subleading. The proton contribution can be neglected because its contribution to $\vec{j}^{(A)}$ is $O(1/m_p)$ and is smaller than the electron contribution by a factor of m_e/m_p . Its contribution to $\rho^{(A)}$ is smaller than the electron contribution by at least 1 power of m_e/m_p in the multiple expansion, because the size of the proton wave function is smaller than that of the electron wave function by a m_e/m_p factor.

After performing the spin sum, contraction of the leptonic and atomic tensors, and implementing the current conservation condition to relate the longitudinal spatial current to the charge density

$$j_{\parallel}^{(A)}(\vec{q}) \equiv \frac{\vec{q}}{q} \cdot \vec{j}^{(A)}(\vec{q}) = \frac{T}{q} \rho^{(A)}(\vec{q}), \quad (9)$$

where $q \equiv |\vec{q}|$, the cross section can be cast into the following form:

$$d\sigma = \frac{\pi}{|\vec{k}_1|} \frac{(4\pi\alpha)^2}{Q^4} \sum_{X=L,T} \left[\left(e_i^2 V_X^{(F_1)} + \frac{\kappa_i^2}{(2m_e)^2} V_X^{(F_2)} \right) R_X \right] \times \frac{d^3\vec{k}_2}{(2\pi)^3 2\omega_2}, \quad (10)$$

through defining the longitudinal and transverse response functions, R_L and R_T , and the corresponding kinematic factors, V_L and V_T . The kinematic factors, which depend on the energy transfer T and momentum transfer q , are

$$V_L^{(F_1)} = \frac{Q^4}{q^4} [(\omega_1 + \omega_2)^2 - q^2], \quad (11)$$

$$V_T^{(F_1)} = - \left[\frac{Q^2(Q^2 + 4\omega_1\omega_2)}{2q^2} + Q^2 + 2m_i^2 \right], \quad (12)$$

and

$$V_L^{(F_2)} = \frac{-Q^4}{q^4} [(\omega_1 + \omega_2)^2 Q^2 + 4m_i^2 q^2], \quad (13)$$

$$V_T^{(F_2)} = \frac{Q^2}{2q^2} [Q^2(Q^2 + 4\omega_1\omega_2) - 4m_i^2 q^2], \quad (14)$$

for couplings with the $F_1^{(l)}$ and $F_2^{(l)}$ form factors, respectively.⁴ The response functions, which are also functions of (T, q) but independent of the form of leptonic coupling, are

⁴As $Q^2 = T^2 - q^2$ and $\omega_2 = \omega_1 - T$, the independent variables in these expressions are thus taken by (T, q) .

$$R_L \equiv \sum_{m_{j_f}} \overline{\sum_{m_{j_i}}} \int \frac{d^3\vec{p}_r}{(2\pi)^3} |\langle f | \rho^{(A)}(\vec{q}) | i \rangle|^2 \delta \left(T - B - \frac{q^2}{2M} - \frac{p_r^2}{2\mu_{\text{red}}} \right), \quad (15)$$

$$R_T \equiv \sum_{m_{j_f}} \overline{\sum_{m_{j_i}}} \int \frac{d^3\vec{p}_r}{(2\pi)^3} |\langle f | j_{\perp}^{(A)}(\vec{q}) | i \rangle|^2 \delta \left(T - B - \frac{q^2}{2M} - \frac{p_r^2}{2\mu_{\text{red}}} \right), \quad (16)$$

where B is the binding energy of the H atom, $M = m_e + m_p \approx m_p$, and $\mu_{\text{red}} = m_e m_p / (m_e + m_p) \approx m_e$. Note that the center-of-mass degrees of freedom in the final state have been integrated out by the momentum conservation, which yield $\vec{p}_R = \vec{q}$; and the resulting energy conservation delta function properly takes care the nuclear recoil effect.

Consider now the ionization of a hydrogenlike atom from its ground state, i.e., the $1s$ orbit, the relevant atomic spatial wave functions for the initial (i) and final (f) states are

$$\langle \vec{r} | i \rangle = \langle \vec{r} | (nlm_l = 100) \rangle = \frac{1}{\sqrt{\pi}} Z^{3/2} e^{-Z\vec{r}}, \quad (17)$$

$$\begin{aligned} \langle f | \vec{r} \rangle &= \langle \vec{r} | \vec{p}_r | \vec{r} \rangle \\ &= e^{\frac{\pi z}{2\bar{p}_r}} \Gamma \left(1 - \frac{iZ}{\bar{p}_r} \right) e^{-i\bar{p}_r \cdot \vec{r}} {}_1F_1 \left(\frac{iZ}{\bar{p}_r}, 1, i(p_r r + \bar{p}_r \cdot \vec{r}) \right), \end{aligned} \quad (18)$$

in atomic units [so the barred quantities are $\bar{r} = rm_e\alpha$, $\bar{p}_r = p_r/(m_e\alpha)$, etc.], where $\Gamma(z)$ and ${}_1F_1(a, b, z)$ are the Gamma and confluent hypergeometric functions, respectively. The evaluations of R_L and R_T can be done analytically by the Nordsieck integration [16–19] and yield

$$R_L = \frac{2^8 Z^6 \bar{q}^2 (3\bar{q}^2 + \bar{p}_r^2 + Z^2) \exp \left[-\frac{2Z}{\bar{p}_r} \tan^{-1} \left(\frac{2Z\bar{p}_r}{\bar{q}^2 - \bar{p}_r^2 + Z^2} \right) \right]}{3((\bar{q} + \bar{p}_r)^2 + Z^2)^3 ((\bar{q} - \bar{p}_r)^2 + Z^2)^3 (1 - e^{-2\pi Z/\bar{p}_r})}, \quad (19)$$

$$\begin{aligned} R_T &= \frac{2^7 \alpha^2 Z^6 (\bar{p}_r^2 + Z^2) \exp \left[-\frac{2Z}{\bar{p}_r} \tan^{-1} \left(\frac{2Z\bar{p}_r}{\bar{q}^2 - \bar{p}_r^2 + Z^2} \right) \right]}{3((\bar{q} + \bar{p}_r)^2 + Z^2)^2 ((\bar{q} - \bar{p}_r)^2 + Z^2)^2 (1 - e^{-2\pi Z/\bar{p}_r})} \\ &\quad + \frac{1}{2} \mu_e^2 \alpha^2 \bar{q}^2 R_L. \end{aligned} \quad (20)$$

The first term in R_T is the contribution from the convection current, and the second one from the spin current. The overall α^2 factor appearing in both terms reflects the $1/m_e^2$ order in the nonrelativistic expansion. In comparison, R_L is $O(\alpha^0)$.

The single differential cross section with respect to the energy transfer can then be computed by integration over the lepton scattering angle θ ,

$$\frac{d\sigma}{dT} = \int d\cos\theta \frac{2\pi\alpha^2}{Q^4} \frac{k_2}{k_1} (V_L R_L + V_T R_T), \quad (21)$$

$$V_{L,T} = e_i^2 V_{L,T}^{(F_1)} + \frac{\kappa_i^2}{(2m_e)^2} V_{L,T}^{(F_2)},$$

with a constrained range of $\cos\theta$:

$$\min\left\{1, \max\left[-1, \frac{k_1^2 + k_2^2 - 2M_H(T-B)}{2k_1 k_2}\right]\right\} \leq \cos\theta \leq 1. \quad (22)$$

For the latter discussion, we note that for a fixed energy transfer, the square of the four-momentum transfer,

$$Q^2 = 2m_i^2 - 2\omega_1(\omega_1 - T) + 2\sqrt{\omega_1^2 - m_i^2}\sqrt{(\omega_1 - T)^2 - m_i^2} \cos\theta, \quad (23)$$

only depends on $\cos\theta$; therefore, the integration over $\cos\theta$ is equivalent to integrating over Q^2 (or q^2).

While it is straightforward to obtain complete and analytic results for ionizations of the hydrogen atom to the order outlined above,⁵ we shall discuss several approximation schemes often employed in atomic calculations, and compare them with the full calculations for this case study in the following sections.

A. Free electron approximation

The FEA is expected to be a good approximation if the photon wavelength is much smaller than the size of the atom (or the typical distance between electrons in a multi-electron system) such that the atomic effect is no longer important. Thus, a necessary (but not sufficient) condition for this approximation to be valid is that the scattering energy needs to be high (compared with the typical scale of the problem).

In this approximation, the electron before and after ionization is treated as a free particle. The free electron cross section of Eq. (1) is multiplied by the step function $\theta(T-B)$ to incorporate the binding effect:

$$\frac{d\sigma}{dT} \Big|_{\text{FEA}} = \theta(T-B) \frac{d\sigma}{dT} \Big|_{\text{FE}}. \quad (24)$$

Energy and momentum conservation fixes $Q^2 = -2m_e T$ in this two-body phase space.

B. Equivalent photon approximation

The equivalent photon approximation [20,21] treats the virtual photon as a real (and thus transversely polarized) photon. It could be a good approximation for low energy processes where the photon is soft such that $Q^2 \approx 0$

because $q^\mu \approx 0$ for every component of μ . At high energies, besides soft photon emissions, when the initial and final state electrons are highly relativistic and almost collinear, the emitted ‘‘collinear’’ photon also has $Q^2 \approx 0$. While the soft photon emission is likely to dominate the phase space of low energy scattering, whether the soft and collinear photon emission will dominate the high energy scattering depends on the transition matrix elements.

The total cross section σ_γ for the photoionization process $\gamma + H \rightarrow H^+ + e^-$ is

$$\sigma_\gamma(T) = \frac{2\pi^2\alpha}{T} R_T^0, \quad (25)$$

where the photon energy $E_\gamma = T$ and the superscript ‘‘0’’ denotes that the photon is ‘‘on shell,’’ i.e., $T^2 = q^2$. Then EPA relates σ_γ to a corresponding lepto-ionization process (involving a virtual photon) by the following two steps: (i) ignoring the longitudinal response function R_L and (ii) substituting the off-shell response function R_T by the on-shell R_T^0 extracted from the photoionization process, i.e.,

$$\begin{aligned} \frac{d\sigma}{dT} \Big|_{\text{EPA}} &= \int d\cos\theta \frac{2\pi\alpha^2}{Q^4} \frac{k_2}{k_1} \left[V_T \left(\frac{T}{2\pi^2\alpha} \sigma_\gamma(T) \right) \right], \\ &\equiv \frac{1}{T} N(T) \sigma_\gamma(T), \end{aligned} \quad (26)$$

with the energy spectrum of an equivalent photon $N(T)$ defined by

$$N(T) = \frac{\alpha}{\pi} \frac{k_2}{k_1} T^2 \int d\cos\theta \frac{V_T}{Q^4}, \quad (27)$$

where the integration range of $\cos\theta$ is the same as Eq. (22). Because it directly feeds the photoionization cross sections (experimental accessible) to the corresponding lepto-ionization cross sections, a lot of theoretical work and uncertainties can be saved when it works properly.

At this point, we should make an important remark regarding the approximation scheme adopted in Ref. [10]: Even though it is in the spirit of the EPA, however, it makes a stronger assumption that the integration leading to the energy spectrum of an equivalent photon is also dominated by the $Q^2 \approx 0$ region (or staying constant), i.e.,

$$N(T) \Big|_{\text{EPA}^*} \approx \frac{\alpha}{\pi} \frac{k_2}{k_1} T^2 \int d\cos\theta \frac{V_T}{Q^4} \Big|_{Q^2 \approx 0}. \quad (28)$$

To distinguish this stronger version of the EPA from the conventional one, we shall denote it as the EPA* scheme.

C. Longitudinal photon approximation

The longitudinal photon contribution is at leading order in the $1/m_e$ expansion while the transverse photon contribution is subleading. Thus, it might be a good approximation for nonrelativistic systems:

⁵Ionizations of hydrogenlike atoms in metastable states can be performed similarly; however, the analytic results get more and more tedious as the principle quantum number n grows.

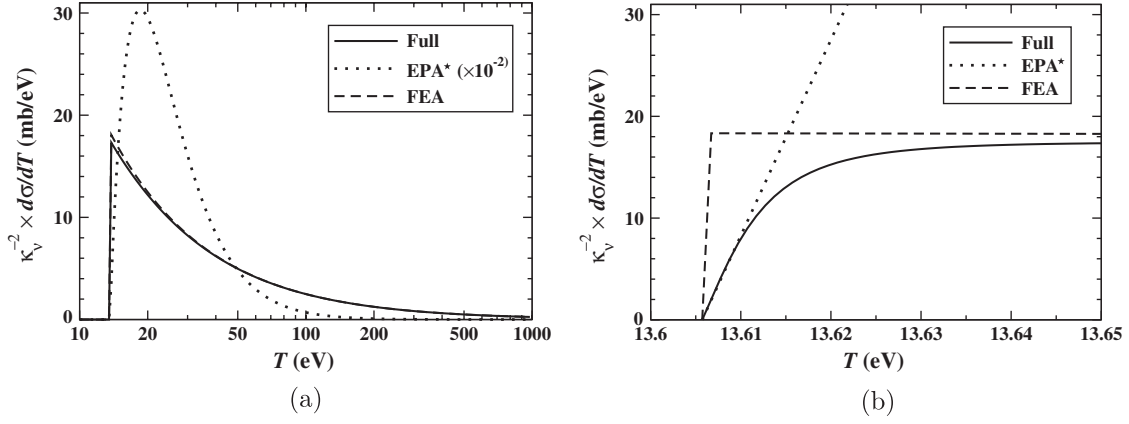


FIG. 2. Differential cross sections $\frac{d\sigma}{dT}$ for $\bar{\nu} + \text{H} \rightarrow \bar{\nu} + p + e^-$ via the EM interaction with the neutrino magnetic moment $\mu_\nu = \kappa_\nu \mu_B$. The incident neutrino has energy $\omega_1 = 1$ MeV with its mass m_ν taken to be zero. The results of the approximation schemes KSV and LPA (both not shown) are in excellent agreement with the full calculation. The kinematic inputs are: (a) $\omega_1 = 1$ MeV, (b) $\omega_1 = 1$ MeV, near threshold T .

$$\left. \frac{d\sigma}{dT} \right|_{\text{LPA}} = \int d\cos\theta \frac{2\pi\alpha^2}{Q^4} \frac{k_2}{k_1} V_L R_L. \quad (29)$$

$$\left. \frac{d\sigma}{dT} \right|_{\text{KSV}} = \int d\cos\theta \frac{2\pi\alpha^2}{Q^4} \frac{k_2}{k_1} \left(V_L + 2 \frac{T^2}{q^2} V_T \right) R_L. \quad (31)$$

The difference of this approximation to the full calculation is a measure of how importantly the transverse current contributes to the process.

D. Approximation scheme of Kouzakov, Studenikin, and Voloshin

The KSV scheme includes the longitudinal photon contribution which is at leading order in the $1/m_e$ expansion and approximates the subleading transverse photon contribution by a relation only strictly suitable for the electric dipole (E_1) transition in the long wavelength limit, i.e., $q \rightarrow 0$:

$$R_T = 2 \frac{T^2}{q^2} R_L. \quad (30)$$

This relation⁶ can be derived from the Siegert theorem [22] for E_1 , which is based on current conservation. It can also be explicitly checked by taking the same limit to Eqs. (19) and (20). In general, R_T is not dominated by E_1 in the processes that we are considering, which requires $qr_A \ll 1$ where r_A is the size of the atom. But Eq. (30) can still be a good approximation to the cross section calculations as long as R_T remains subleading to R_L .

In Refs. [12,13], the authors adopted the above relation so the cross section was calculated without need to evaluate the transverse response function which is harder to compute:

⁶Note that the factor of 2 difference from Eq. (12) of Ref. [13] is due to the different definitions for the transverse response function.

III. IONIZATION BY NEUTRINO MAGNETIC MOMENT

In case the incident lepton is a neutrino (ν) or antineutrino ($\bar{\nu}$), as $e_\nu = 0$, the EM breakup process is thus sensitive to the neutrino magnetic moment $\mu_\nu = \kappa_\nu \mu_B$ (which is purely anomalous). The energy spectrum for reactor antineutrinos typically peaks around a few tens of keV to MeV (see, e.g., Ref. [5]); setting $\omega_1 = 1$ MeV, a plot of the single differential cross section with energy loss up to 1 keV is given in Fig. 2. Not shown in these figures are the results of the approximation schemes KSV and LPA. They both agree with the full calculation to good extents: within 10^{-5} for the former and 10^{-3} for the latter in the entire range. In other words, this atomic bound-to-free transition is dominated by the atomic charge operator, while the transverse current operator is negligible, which implies the inadequacy of the EPA scheme.

The dominance of the charge operator over the transverse current can be roughly understood by a comparison of their corresponding kinematic factors $V_L^{(F_2)}$ and $V_T^{(F_2)}$. For neutrino scattering

$$Q^2 \Big|_{m_\nu=0} \approx -2\omega_1^2(1-x), \quad (32)$$

where $x \equiv \cos\theta$; they are

$$\frac{V_L^{(F_2)}}{Q^4} = \frac{2(1-x)}{\left(1-x + \frac{T^2}{2\omega_1^2}\right)^2}, \quad \frac{V_T^{(F_2)}}{Q^4} = \frac{(1+x)}{2\left(1-x + \frac{T^2}{2\omega_1^2}\right)}. \quad (33)$$

As $T^2/\omega_1^2 \ll 1$ in our consideration, both functions peak near $x = 1$, and they have similar maximum values:

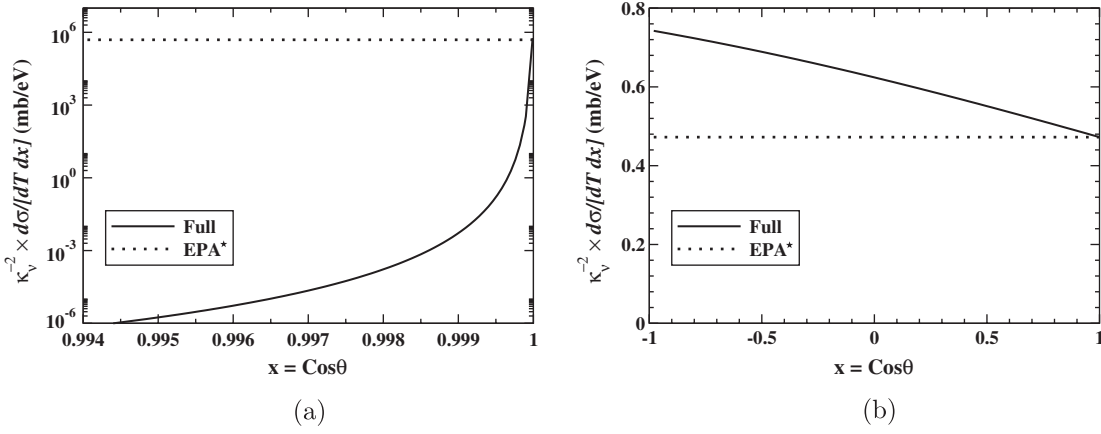


FIG. 3. Double differential cross sections $\frac{d^2\sigma}{dTdx}$ for $\bar{\nu} + H \rightarrow \bar{\nu} + p + e^-$ via the EM interaction with the neutrino magnetic moment μ_ν . The energy transfer is fixed at 20 eV. EPA* hugely overestimates at high ω_1 , but works reasonably at low ω_1 . The kinematic inputs are: (a) $\omega_1 = 1$ MeV, $T = 20$ eV, (b) $\omega_1 = 1$ keV, $T = 20$ eV.

$V_L^{(F_2)}/Q^4|_{\max} = \omega_1^2/T^2$ and $V_T^{(F_2)}/Q^4|_{\max} = 2\omega_1^2/T^2$, and widths. Since the transverse response function does not get enhancement from the kinematic factor $V_T^{(F_2)}$ over $V_L^{(F_2)}$, its contribution to the cross section is suppressed by the usual nonrelativistic order α^2 .

The good agreements with the FEA scheme [Fig. 2(a)] are not really a surprise: The energetic neutrino emits a virtual photon with a wavelength smaller than the atomic size so that the binding effect does not manifest in a short distance. The only exception is near the ionization threshold [Fig. 2(b)] where the virtual photon wavelength is larger than the atomic size, and the binding effect suppresses the cross section in comparison to FEA.

Also shown in these figures is the result of the EPA* scheme. Note that the curve in Fig. 2(b) has to be scaled down by a factor of 100 in order to be cast on the same plot as other calculations; in other words, the EPA* hugely overestimates the cross section by several orders of magnitude. There is only a tiny region near the ionization

threshold [see Fig. 2(a)] where the EPA* does work; that is where the virtual photon approaches the real photon limit ($T = q$). The origin of such an overestimation can be clearly seen in Fig. 3(a), where the double differential cross section $d\sigma/(dTdx)$ is plotted as a function of x with a fixed energy loss $T = 20$ eV. Because of the kinematic constraint, the maximum scattering angle $\theta_{\max} = 6.28^\circ$. However, even within this small range of the peripheral scattering angle, the differential cross section decreases dramatically by 12 orders of magnitude from the forward angle as a combined result of the kinematic factors $V_{L,T}$ and the response functions $R_{L,T}$. Therefore, the flatness of $d\sigma/(dTdx)$ required by the EPA* is severely violated and results in this overestimation.

On the other hand, one does see the EPA* start to work when the incident neutrino energy ω_1 drops below the binding momentum of the hydrogenlike atom $\sim Zm_e\alpha$. For hydrogen, the scale is about 3.73 keV, and Fig. 4 shows that varying ω_1 from 3 and 2 to 1 keV, the EPA* result

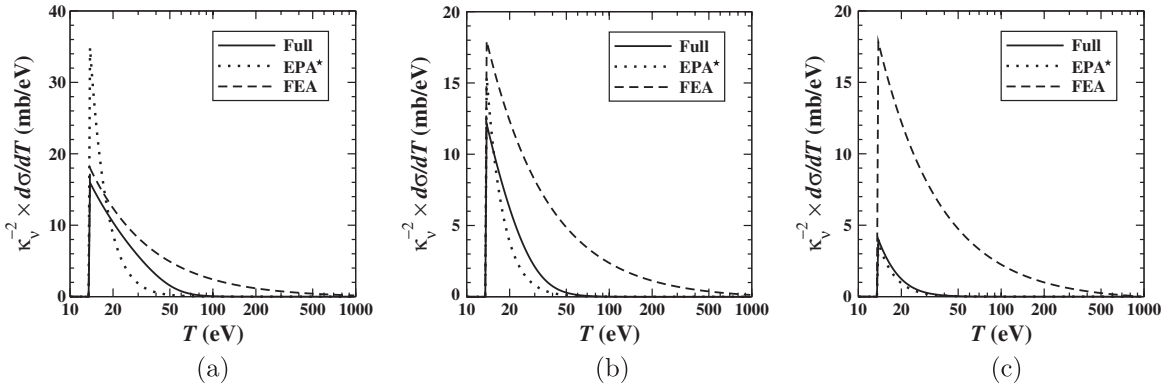


FIG. 4. Differential cross sections $\frac{d^2\sigma}{dTdx}$ for $\bar{\nu} + H \rightarrow \bar{\nu} + p + e^-$ via the EM interaction with the neutrino magnetic moment μ_ν at a few keV incident energies. The EPA* calculations gradually converge to the full ones. The kinematic inputs are: (a) $\omega_1 = 3$ keV, (b) $\omega_1 = 2$ keV, (c) $\omega_1 = 1$ keV.

becomes reasonably good. As evidenced from Fig. 3(b), the double differential cross section for $\omega_1 = 1$ keV and $T = 20$ eV, even though not looking completely flat, does vary only modestly with increasing θ , and the agreement is getting better when ω_1 is further decreased. In the meanwhile, the FEA is no longer a good approximation since the de Broglie wavelength of the incident neutrino is on the order of atomic size so the binding effect is not negligible.

IV. IONIZATION BY MUON

Replacing the incident lepton from a neutrino to a muon (μ^-), as $e_{\mu^-} = -1$, the EM breakup process is instead dominated by the F_1 coupling, while the F_2 coupling can be ignored for the smallness of muon $g - 2 \approx 0.001$ [1]. Consider relativistic muons with $10^{0,1,2,3}$ GeV energies, the differential cross sections are plotted in Fig. 5. (Because the muon is relativistic while the electron is nonrelativistic, the final state interaction between the muon and electron can be ignored; see, e.g., Ref. [23].) The noticeable differences in comparison to what have been drawn in the previous neutrino case are (1) The differential cross section falls off more quickly as T

increases, i.e., the recoil electrons tend to have relatively smaller energies. (2) The FEA results are insensitive to ω_1 and largely underestimated in all cases. (3) There are substantial contributions from the transverse current, despite its built-in $O(Z^2\alpha^2)$ suppression due to the nonrelativistic kinematics of atomic electrons. In fact, when ω_1 becomes big enough, the interaction with the atomic transverse current dominates over the one with the charge and longitudinal current, as indicated by the competition between the EPA and the LPA curves in Fig. 5, and one expects the larger ω_1 increases, the better the EPA works.

The reason for such differences is primarily due to the associated kinematic factors. At the $Q^2 \rightarrow 0$ limit, they behave like $V_L^{(F_1)} \propto Q^4$ and $V_T^{(F_1)} \propto Q^0$ for muon ($m_\mu \neq 0$), and $V_L^{(F_2)} \propto Q^6$ and $V_T^{(F_2)} \propto Q^4$ for neutrino ($m_\nu \approx 0$) ionization, respectively. As the differential cross section $d\sigma/dT$ involves a $1/Q^4$ weighted integration over Q^2 , only the transverse part in muon ionization receives a strong weight at peripheral scattering angles (where $Q^2 \approx 0$). This explains the importance of the transverse current in relativistic muon ionization and its insignificance in neutrino ionization. Also, with the allowed scattering angles becoming closer to the exact forward

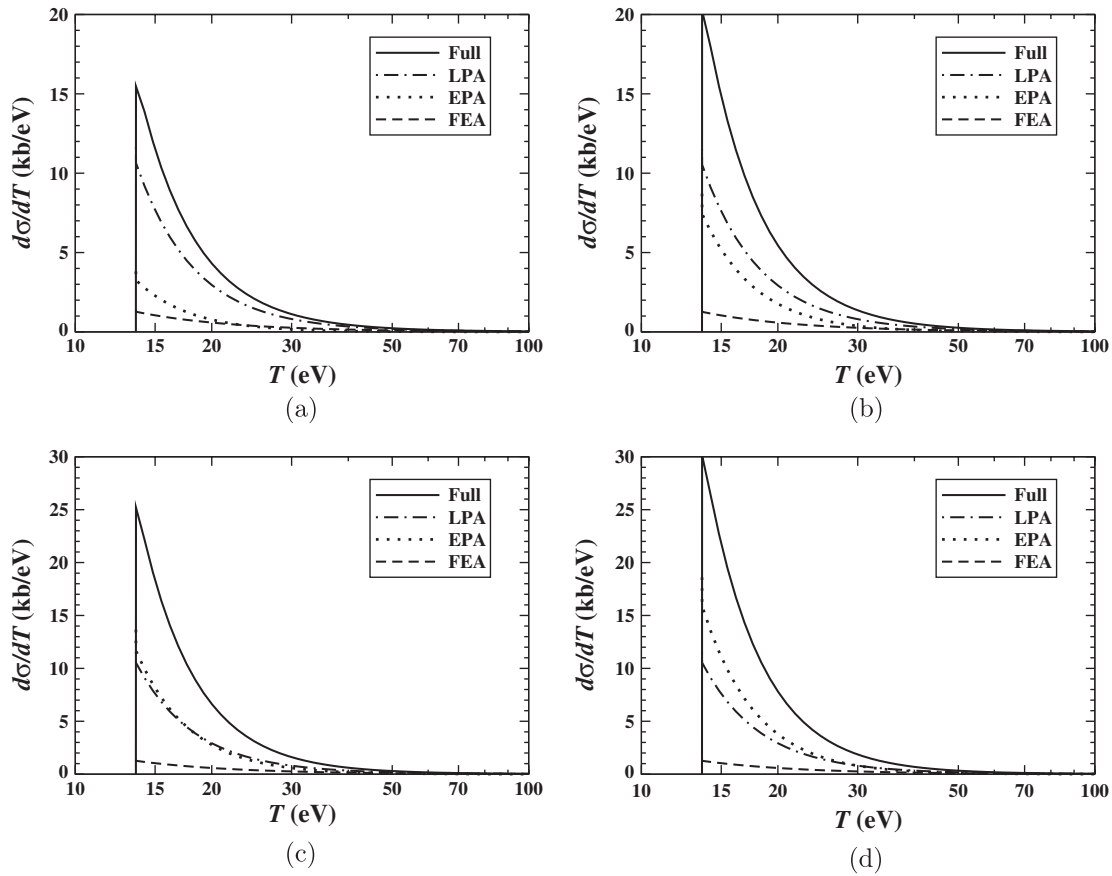


FIG. 5. Differential cross sections $\frac{d\sigma}{dT}$ for $\mu^- + \text{H} \rightarrow \mu^- + p + e^-$ via the EM interaction. The results of the approximation schemes KSV (not shown) are in excellent agreement with the full calculation. The kinematic inputs are: (a) $\omega_1 = 1$ GeV, (b) $\omega_1 = 10$ GeV, (c) $\omega_1 = 100$ GeV, (d) $\omega_1 = 1000$ GeV.

direction as the muon incident energy increases (with T fixed), the kinematics becomes real-photon-like and eventually the huge enhancement by the $1/Q^4$ weight is able to overcome the nonrelativistic suppression in the transverse response function. The failure of the FEA in relativistic muon ionization can also be understood in a similar way: In the FEA scheme, the differential cross section $d\sigma/dT$ is determined from a specific kinematics $Q_{\text{FEA}}^2 = -2m_e T$ by energy-momentum conservation; on the other hand, the full calculation with two-body kinematics involves an integration over allowed $|Q^2|$ ranging from ≈ 0 to some maximum value determined by the maximum scattering angle. Because the $1/Q^4$ factor that enhances the contributions from the $Q^2 \approx 0$ region, the $Q_{\text{FEA}}^2 = -2m_e T$ ceases to be a good representative point.

A semiquantitative understanding could be obtained by the following approximate forms of $V_L^{(F_1)}$ and $V_T^{(F_1)}$. For a relativistic muon,

$$Q^2|_{\omega_1 \gg m_\mu} \approx -2\omega_1^2(1-x) - m_\mu^2 \frac{T^2}{\omega_1^2}, \quad (34)$$

they are

$$\begin{aligned} \frac{V_L^{(F_1)}}{Q^4} &= \frac{1}{2\omega_1^2} \frac{(1+x)}{\left(1-x + \frac{T^2}{2\omega_1^2}\right)^2}, \\ \frac{V_T^{(F_1)}}{Q^4} &= \frac{1}{4\omega_1^2} \frac{(1-x)(3-x) + (3+x)\frac{m_\mu^2}{\omega_1^2} \frac{T^2}{2\omega_1^2}}{\left(1-x + \frac{T^2}{2\omega_1^2}\right)\left(1-x + \frac{m_\mu^2}{\omega_1^2} \frac{T^2}{2\omega_1^2}\right)^2}. \end{aligned} \quad (35)$$

One sees that unlike the previous case for which $V_T^{(F_2)}$ and $V_L^{(F_2)}$ are comparable in most of the range of x , $V_T^{(F_1)}/Q^4$ is comparable to $V_L^{(F_1)}/Q^4$ only for $1-x \gtrsim \frac{T^2}{2\omega_1^2}$. As the scattering angle further decreases, $V_T^{(F_1)}/Q^4$ starts to dominate over $V_L^{(F_1)}/Q^4$, and when $1-x \lesssim \frac{m_\mu^2}{\omega_1^2} \frac{T^2}{2\omega_1^2}$, it overwhelms by a factor $\frac{\omega_1^2}{m_\mu^2} \gg 1$. Also, because of this huge weight on extremely small angles, the FEA scheme with $|Q_{\text{FEA}}^2| = 2m_e T$ overestimates the averaged $|Q^2|$ for the realistic situation and leads to an underestimation.

Though one sees that the EPA serves as a better approximation than the FEA in the relativistic muon ionization, however, as shown in Fig. 5, even at $\omega_1 = 1000$ GeV, it can still not be taken as a good approximation to the full result. The main reason is its nonzero mass which limits the lowest $|Q^2|$ to be reached:

$$|Q^2|_{\min} \approx \frac{T^2}{\omega_1^2} m_\mu^2 |_{\omega_1 \gg m_\mu \gg T}. \quad (36)$$

If m_μ is adjusted to smaller values $\lesssim 1$ eV, then indeed the EPA accounts for $\gtrsim 80\%$ of the differential cross section for ω_1 on the orders of GeV–TeV with $T = 15$ eV, as shown in Fig. 6. In other words, in case one seeks a better description of relativistic muon ionization or other

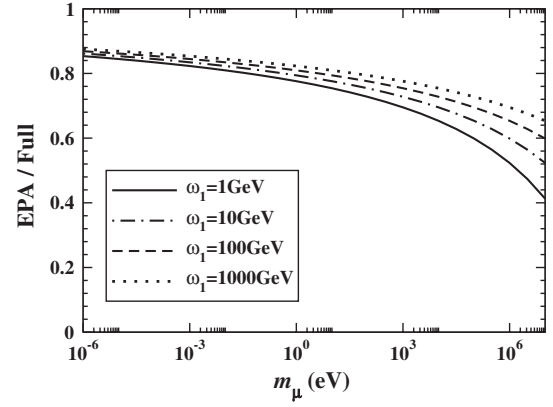


FIG. 6. The EPA scheme as an approximation for the relativistic muon ionization with an adjustable m_μ for $d\sigma/dT$ with $T = 15$ eV.

processes alike beyond the EPA, the contribution from charge and longitudinal current should be included.

V. IONIZATION BY WIMP

Instead of a relativistic muon, consider now the atomic ionization by some nonrelativistic, weakly interacting massive particle, χ , which could be a DM candidate. Suppose this particle is of galactic origin with a mean velocity $v_\chi \sim 220/(3 \times 10^5)$, its kinetic energy $\approx \frac{1}{2} m_\chi v_\chi^2 = 270 \left(\frac{m_\chi}{\text{GeV}}\right) \text{ eV}$; therefore, in order to ionize a hydrogen, $m_\chi \gtrsim 60$ MeV. To make use of the general formalism developed in Sec. II, we postulate a QED-like fermionic DM-electron (χe) interaction in which the new $U(1)$ gauge boson has mass m_b and the interaction strength $\alpha_{\chi e} \equiv g_{\chi e} \alpha$. Figure 7 shows the differential cross sections for $m_\chi = 100$ MeV and 1 GeV, with either a massless gauge boson $m_b = 0$, which corresponds to an infinitely long-ranged interaction, or a very massive one $m_b = 125$ GeV, which leads to an extremely short-ranged interaction.⁷

Not shown in Figs. 7(a)–7(d) are the results of the KSV and LPA, as they are in excellent agreement with the full calculations in all cases illustrated. Accordingly, the failure of the EPA scheme is anticipated. On the other hand, although it is expected that the binding effect should suppress the FEA results, the several orders of magnitude overestimation by the FEA scheme in the entire range of the energy transfer, evidenced in panels (a)–(d), indicates the inadequacy of the FEA scheme in such a kinematic regime. Figures 7(e) and 7(f) show that the differential cross section becomes “saturated” when m_χ becomes much bigger than 1 GeV, which is about the mass of the hydrogen target. This can be understood by transforming the laboratory frame, where the hydrogen target is

⁷Note that the coupling strength $g_{\chi e}$ is associated with the choice of m_b .

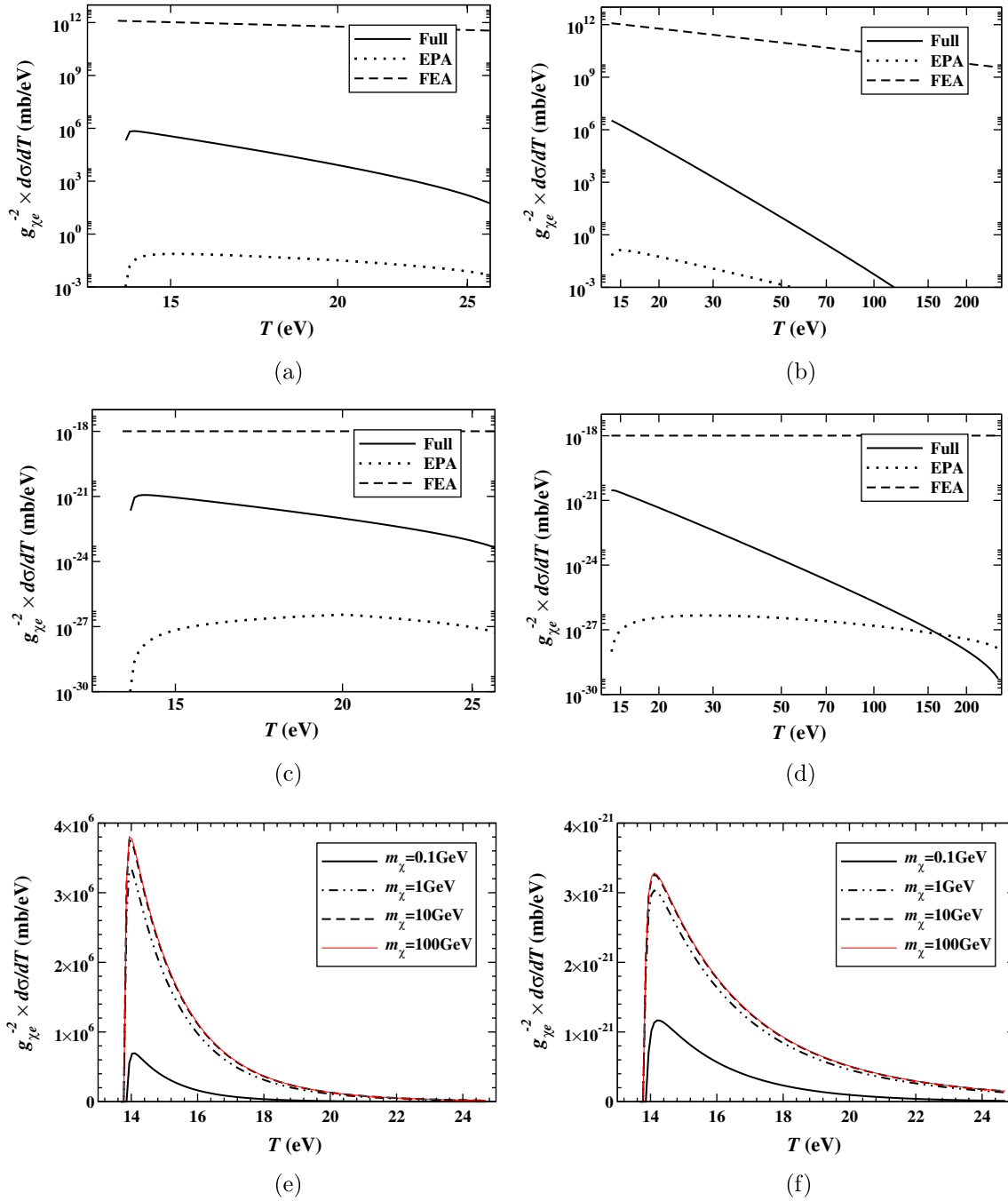


FIG. 7 (color online). Differential cross sections $d\sigma/dT$ for $\chi + H \rightarrow \chi + p + e^-$ via a QED-like χe interaction with the $U(1)$ gauge boson of mass m_b and interaction strength $g_{\chi e}\alpha$. The results of the approximation schemes KSV and LPA [not shown in (a)–(d)] are in excellent agreement with the full calculation, and only the full results are shown in (e) and (f). The kinematic inputs are: (a) $m_\chi = 0.1$ GeV, $m_b = 0$, (b) $m_\chi = 1$ GeV, $m_b = 0$, (c) $m_\chi = 0.1$ GeV, $m_b = 125$ GeV, (d) $m_\chi = 1$ GeV, $m_b = 125$ GeV, (e) $m_b = 0$, near threshold, (f) $m_b = 125$ GeV, near threshold.

stationary, to the DM rest frame which coincides with the center-of-mass frame for $m_\chi \gg m_p$: The kinematics only depends on v_χ and the reduced mass $\approx m_p$. Also by comparing the case with $m_b = 0$, Figs. 7(a), 7(b), and 7(e)

and $m_b = 125$ GeV, Figs. 7(b), 7(d), and 7(e), the differential cross sections, apart from some overall scale factors, show a slower decreasing with energy transfer T as the range of the χe interaction decreases.

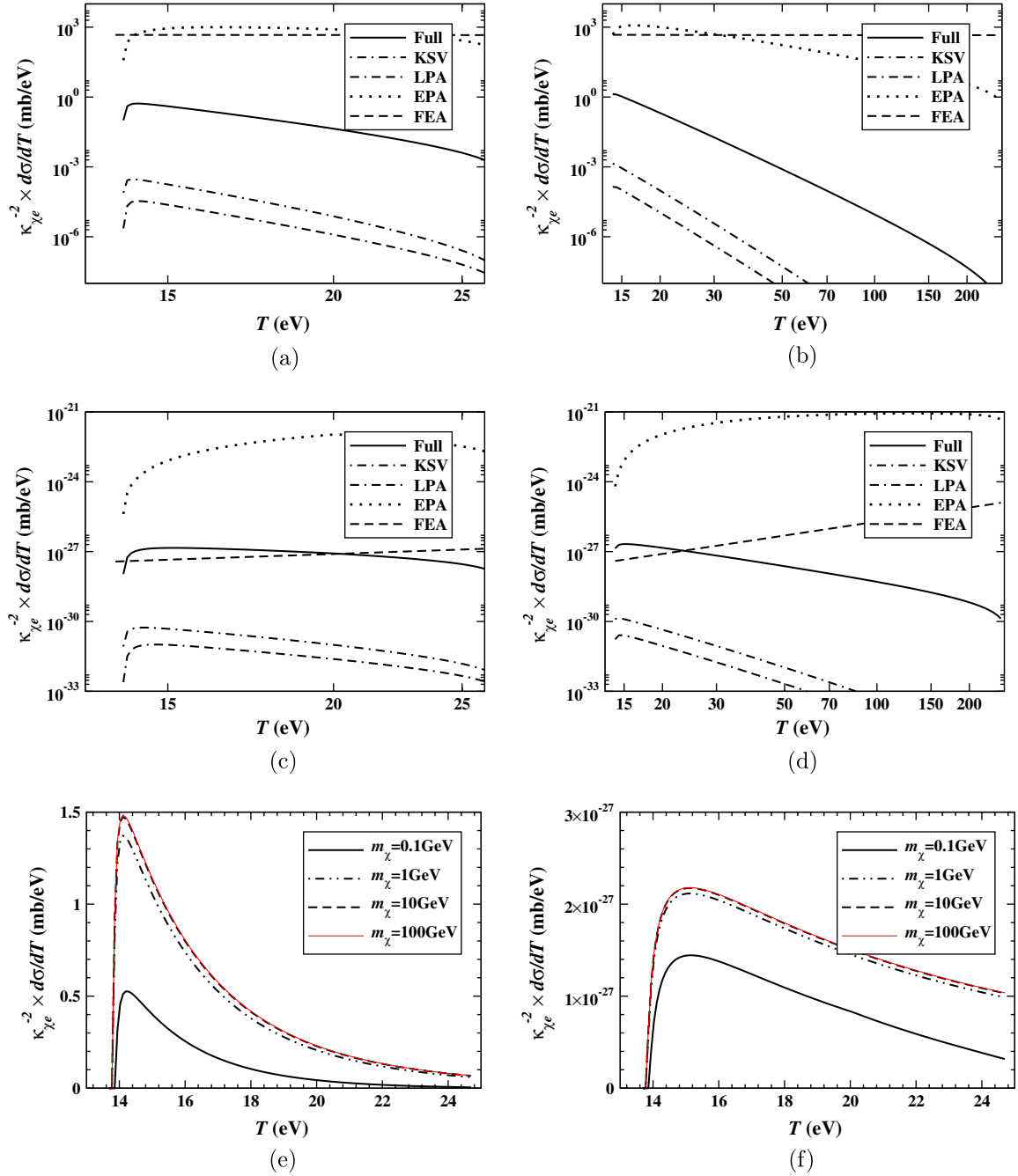


FIG. 8 (color online). Differential cross sections $d\sigma/dT$ for $\chi + H \rightarrow \bar{\nu} + p + e^-$ via an anomalous-magnetic-moment-like χe interaction with the $U(1)$ gauge boson of mass m_b and coupling strength $\kappa_{\chi e} \alpha$. Only the full results are shown in (e) and (f). The kinematic inputs are: (a) $m_\chi = 0.1$ GeV, $m_b = 0$, (b) $m_\chi = 1$ GeV, $m_b = 0$, (c) $m_\chi = 0.1$ GeV, $m_b = 125$ GeV, (d) $m_\chi = 1$ GeV, $m_b = 125$ GeV, (e) $m_b = 0$, near threshold, (f) $m_b = 125$ GeV, near threshold.

If, on other hand, the neutral fermionic dark matter has a nonzero (anomalous) magnetic moment, or its coupling to the $U(1)$ gauge boson is via the Dirac bilinear $\bar{\chi} \sigma_{\mu\nu} q^\nu \chi / (2m_\chi)$, a different constant $\alpha_{\chi e} = \kappa_{\chi e} \alpha$ is assigned to characterize the interaction strength. This anomalous-magnetic-moment-like interaction yields quite different results, as shown in Fig. 8, from the previous case with the same kinematics. The most noticeable difference

seen in Figs. 8(a)–8(d) is that the KSV and LPA no longer work, and in fact, largely underestimate. This implies not only substantial contributions from the transverse response but also the breakdown of the long wavelength approximation, which has been good for all cases previously discussed. However, the EPA does not work either: It yields a huge overestimation which implies that the transverse kinematics is not dominated by the photonlike

$Q^2 \approx 0$ region. Therefore, one encounters a very subtle kinematic regime where none of the approximation schemes work and requires a full calculation. While Figs. 8(e) and 8(f) show a similar cross section saturation for $m_\chi \gg m_p$ and the range effect on the differential cross section as previously found, a comparison of Figs. 7 and 8 shows that the large energy transfer regime is more suppressed in the QED-like interaction than the anomalous-magnetic-moment-like interaction.

The general trend observed above for the χe cross sections that the atomic charge operator dominates in the QED-like interaction while the transverse current operator dominates in the anomalous-magnetic-moment-like interaction is opposite to what has been concluded for the ionizations by relativistic muons (F_1 coupling) and neutrinos (F_2 coupling). This difference is also partially due to the corresponding kinematic factors: With $m_\chi^2 \gg |Q^2|, q^2, T^2$, they are

$$V_L^{(F_1)} \approx 4m_\chi^2 \frac{Q^4}{q^4}, \quad V_T^{(F_1)} \approx 2m_\chi^2 \left(\frac{|Q^2|}{2m_\chi^2} - \frac{T^2}{q^2} \right), \quad (37)$$

and

$$V_L^{(F_2)} \approx 4m_\chi^2 \frac{Q^4}{q^4} \left(\frac{\omega_1 T}{m_\chi^2} |Q^2| - T^2 \right), \quad (38)$$

$$V_T^{(F_2)} \approx 2m_\chi^2 |Q^2| \left(1 + \frac{|Q^2|}{q^2} \right).$$

The square of the four-momentum transfer in DM scattering is

$$Q^2 \approx -(2 - r_E - 2\sqrt{1 - r_E x})m_\chi^2 v_\chi^2, \quad (39)$$

where r_E is the fraction of the DM kinetic energy transfer to the atom, i.e., $2T/(m_\chi v_\chi^2)$. For most of the range of x (which is less restricted unless $m_\chi \gg m_p$) and r_E (which can never be zero for ionization), one can estimate $|Q^2| \sim m_\chi^2 v_\chi^2$. Because $T^2 = (r^2 v_\chi^2/4)m_\chi^2 v_\chi^2$, $q^2 = T^2 + |Q^2| \sim m_\chi^2 v_\chi^2$. Using these estimates, the leading orders in v_χ are $O(1)$ for $V_L^{(F_1)}$, $O(v_\chi^2)$ for $V_L^{(F_1)}$, and $O(v_\chi^4)$ for $V_L^{(F_2)}$, $O(v_\chi^2)$ for $V_T^{(F_2)}$, respectively. Therefore,

in ratio to the charge operator, the transverse current is suppressed by $O(v_\chi^2)/O(1)$ in the F_1 -type coupling, while it is enhanced by $O(v_\chi^2)/O(v_\chi^4)$ in the F_2 -type coupling due to the kinematic factors.

VI. CONCLUSION

We studied the ionization of hydrogen by the scattering of the neutrino magnetic moment, relativistic muon, and weakly interacting massive particle with a QED-like interaction. Analytic results were obtained and compared with several approximation schemes often used in atomic physics. It is found that for the case of the neutrino magnetic moment, the atomic charge operator dominates the process, and for typical reactor neutrino energies about tens of keV to a few MeV, the atomic binding effect is negligible. For relativistic muon scattering, on the other hand, the transverse current operator becomes dominant with increasing incident muon energy. In this case, the equivalent photon approximation yields a reasonable result; however, for further improvement, the contribution from the charge operator needs to be taken into account. Also, due to the special weight by kinematics, the free electron approximation largely underestimates the result. The WIMP scattering is the most kinematics-sensitive case, and the free electron approximation fails badly. Depending on the coupling to the dark matter particle, the cross section is dominated by the charge operator for the F_1 coupling, and the transverse current operator for the F_2 coupling. While the longitudinal photon approximation works for the former, none of the approximations under study work for the latter.

ACKNOWLEDGMENTS

We thank Henry T. Wong for stimulating discussions and comments. The work is supported in part by the NSC of ROC under Grants No. 99-2112-M-002-010-MY3, No. 102-2112-M-002-013-MY3 (J. W. C., C. F. L., C. L. W.), No. 98-2112-M-259-004-MY3, and No. 101-2112-M-259-001 (C. P. L.).

-
- [1] J. Beringer *et al.* (Particle Data Group), *Phys. Rev. D* **86**, 010001 (2012).
 [2] C. Brogini, C. Giunti, and A. Studenikin, *Adv. High Energy Phys.* **2012**, 459526 (2012).
 [3] V. N. Aseev *et al.* (Troitsk Collaboration), *Phys. Rev. D* **84**, 112003 (2011).
 [4] A. G. Beda, V. B. Brudanin, V. G. Egorov, D. V. Medvedev, V. S. Pogosov, E. A. Shevchik, M. V. Shirchenko, A. S. Starostin, and I. V. Zhitnikov, *Phys. Part. Nucl. Lett.* **10**, 139 (2013).
 [5] H. T. Wong *et al.* (TEXONO Collaboration), *Phys. Rev. D* **75**, 012001 (2007).
 [6] C. Arpesella *et al.* (The Borexino Collaboration), *Phys. Rev. Lett.* **101**, 091302 (2008).
 [7] P. Vogel and J. Engel, *Phys. Rev. D* **39**, 3378 (1989).

- [8] H. T. Wong, *J. Phys. Conf. Ser.* **309**, 012024 (2011).
- [9] Q. Yue and H. T. Wong, *Mod. Phys. Lett. A* **28**, 1340007 (2013).
- [10] H. T. Wong, H.-B. Li, and S.-T. Lin, *Phys. Rev. Lett.* **105**, 061801 (2010); arXiv:1001.2074v3.
- [11] M. B. Voloshin, *Phys. Rev. Lett.* **105**, 201801 (2010); **106**, 059901(E) (2011).
- [12] K. A. Kouzakov and A. I. Studenikin, *Phys. Lett. B* **696**, 252 (2011).
- [13] K. A. Kouzakov, A. I. Studenikin, and M. B. Voloshin, *Phys. Rev. D* **83**, 113001 (2011).
- [14] R. Essig, J. Mardon, and T. Volansky, *Phys. Rev. D* **85**, 076007 (2012).
- [15] R. Essig, A. Manalaysay, J. Mardon, P. Sorensen, and T. Volansky, *Phys. Rev. Lett.* **109**, 021301 (2012).
- [16] A. Nordsieck, *Phys. Rev.* **93**, 785 (1954).
- [17] A. R. Holt, *J. Phys. B* **2**, 1209 (1969).
- [18] D. Belkić, *J. Phys. B* **14**, 1907 (1981).
- [19] M. S. Gravielle and J. E. Miraglia, *Comput. Phys. Commun.* **69**, 53 (1992).
- [20] C. F. von Weizsacker, *Z. Phys.* **88**, 612 (1934).
- [21] E. J. Williams, *Phys. Rev.* **45**, 729 (1934).
- [22] A. J. F. Siegert, *Phys. Rev.* **52**, 787 (1937).
- [23] L. D. Landau and L. M. Lifshitz, *Quantum Mechanics: Nonrelativistic Theory* (Butterworth-Heinemann, Washington, DC, 1981), 3rd ed.